Proceedings of the ASME 2021
Internal Combustion Engine Division Fall Technical Conference
ICEF2021
October 13-15, 2021, Virtual, Online

ICEF2021-67745

LES STUDY ON SPRAY COMBUSTION WITH RENEWABLE FUELS UNDER ECN SPRAY-A CONDITIONS

Daniel Mira*
CASE Department
Barcelona Supercomputing Center (BSC)
Barcelona, Spain

Eduardo J. Pérez-Sánchez
CASE Department
Barcelona Supercomputing Center (BSC)
Barcelona, Spain

Anurag Surapaneni
CASE Department
Barcelona Supercomputing Center (BSC)
Barcelona, Spain

Jesús Benajes
CMT-Motores Térmicos,
Universitat Politècnica de
València, Spain

José M. García-Oliver†
CMT-Motores Térmicos,
Universitat Politècnica de
València, Spain

José M. Pastor
CMT-Motores Térmicos,
Universitat Politècnica de
València, Spain

Daiana De León
CMT-Motores Térmicos,
Universitat Politècnica de
València, Spain

ABSTRACT

Poly-Oxymethylene Dimethyl Ethers (OMEx) are being intensively investigated because of their potentially renewable synthesis path, which make them suitable as liquid fuels for low-carbon transport applications. In the present contribution, a computational study on the difference in combustion characteristics between dodecane and OMEx-type fuels under Engine Combustion Network (ECN) Spray A conditions is reported. In particular, a blend of different OMEx fuels have been investigated and compared to dodecane, which is a more conventional diesel-like fuel. The modelling framework consists of a high-fidelity LES approach together with a Eulerian-Lagrangian spray model and flamelet-based turbulent combustion model. Results indicate ignition delay time and lift-off length according to the fuel

*Corresponding author: daniel.mira@bsc.es.
†Corresponding author: jgarciao@mot.upv.es.

reactivity properties, with the OMEx fuel performing similarly to dodecane. Flamelet calculations show that ignition of the oxygenated fuels is in general similar to that of dodecane, but it occurs at higher mixture fraction values due to the differences in stoichiometry. One of the most relevant outcomes of the study is the important effect that the oxygenated characteristics of OMEx has on the flame structure. Results show that for OMEx the reaction front is stabilized at distances closer to the nozzle than for dodecane, and that the flame shape as well as its internal structure is clearly affected.

Keywords: Poly-Oxymethylene Dimethyl Ethers ; ECN; Spray A; LES; flamelet.

INTRODUCTION

The need to reduce the effects of the pollutant emissions and greenhouse gas effects from combustion systems has stimulated intensive research in the scientific community. Among the many research lines [1], synthetic fuels obtained from renewable energy sources, have emerged as an attractive solution to contribute to the decarbonization of the transportation sector [2]. These electrofuels or e-fuels are synthesized from hydrogen obtained by electrolysis with renewable electricity and, aside from being used to balance the grid during off-peak periods, they are aimed at replacing fossil fuel sources in propulsion systems. However, they have to meet certain requirements in terms of engine operation and combustion performance and this is still an open research topic.

In this context, oxygenated fuels based on oxymethylene-dimethyl ethers (OMEx) appear as an interesting alternative to reduce soot formation in spray flames [3,4]. OMEx already contains oxygen in the fuel compounds, so they need less mixing to achieve burning conditions and displace combustion to leaner conditions. Additionally, with the absence of C-C bonds there is an overall reduction in soot formation in the flame.

Compared to other oxygenated fuels such as alcohols, OMEx present a much higher oxygen content as well as higher cetane numbers, making them more suitable for current compression ignition (CI) engine architectures. In this sense, research on OMEx has shown a clear and steady growth during the last decade [4]. Published works indicate that the research on these fuels is diverse, with publications mainly being associated with production, engine performance, environmental impact and political and economic implications. Starting from engine-related investigations [5–8], which indicate that these fuels can be a good alternative to fossil fuels, experimental studies have moved towards more fundamental works [9–11], as fundamental knowledge on the flame structure is needed. Currently, many efforts are focused on improving chemical mechanisms [12, 13] and computational fluid dynamics models [9, 14] to deliver more accurate predictions on the combustion behaviour of these fuels.

In this study, the Spray A nominal condition from the Engine Combustion Network (ECN) [15] is used to evaluate the performance of calculation models to predict the combustion behaviour of OMEx-type fuels. Spray A is an interesting test case, as it is representative of the operation conditions of current CI engines. The simplified configuration allows discarding additional phenomena that can complicate fundamental analysis of the spray flame. Spray A has been deeply studied using dodecane as fuel through experiments [16–19] as well as Computational Fluid Dynamics (CFD) simulations using flamelets, Conditional Moment Closure (CMC) and Transported Probability Density Functions (TPDF) models [20–22], in a wide range of conditions. The large amount of results provided a clear picture of the underlying phenomena, with special attention to the analysis of the combustion structure at the lift-off length (LOL) and flame stabilization mechanisms as well as soot formation [19, 23, 24]. However, there is a need to expand the research and gain insights on the physical and chemical interactions in high-pressure spray flames with new fuels such as OMEx, following recent research [9–11, 14].

This study is focused on gaining further insights into the flame structure of high pressure spray flames of OMEx at the nominal condition of the ECN Spray A. The work includes a systematic analysis of the flame structure from laminar to turbulent regimes using high-fidelity simulations coupled to a tabulated chemistry method. Such goal is decomposed into the study of auto-ignition and flame propagation and the description of the flame structure in physical and mixture fraction spaces. To provide a clearer picture, and due to its relevance and abundant literature, dodecane is taken as a reference. The analysis evidences the differences in flame structure between OMEx and dodecane from the perspective of the laminar flame structure and turbulent spray development. Finally, the numerical results are compared with the experiments carried out at the CMT Motores Termicos facility [10, 11].

The paper is structured as such, first, the boundary conditions of the sprays are presented and the computational models are described. This is followed by an analysis of the flame structure using unsteady counterflow diffusion flames and the flamelet method. The thermochemical database generated with the flamelet model is used to describe the turbulent spray flames for the different fuels. Subsequently, a validation of the spray flame for both fuels is given in the next subsection, followed by an analysis of the quasi-steady flame regime with attention to species distribution in respective mixture fraction-temperature maps. Finally, conclusions and outlook close the paper.

CASE DESCRIPTION

The current work aims to compare an oxygenated e-fuel with a reference fuel n-dodecane at the nominal conditions of the Spray A of the Engine Combustion Network (ECN) [15]. Following previously reported experiments [10, 11], a representative

OMEx fuel was chosen, which is made up of blends of different single-component fuels with a generic molecular formula of CH_3O-(CH_2O)n-CH_3 (where n varies between 3 and 5) and a composition of 57.9, 28.87 and 10.08% for OME3, OME4 and OME5, respectively. However, regarding the simulations, as the chemical mechanism does not contain OME5, its corresponding composition has been added to that of OME4 due to the similarity in the chemistry of the molecules [13].

The boundary conditions for the simulation correspond to those from the nominal condition for spray A, that is, 900 K air temperature, 15% in volume of oxygen in air and an air density of 22.8 kg/m^3 [15]. Fuel is injected at 150 MPa at a temperature of 363 K through a nozzle of 90 μm nominal diameter with a discharge coefficient of 0.9 (nozzle 210675) and an injection rate longer than 4 ms to reach quasi-steady state.

The computational domain is represented by a cylinder of radius 23.5 mm and height 108 mm discretized as a structured O-grid mesh. It contains a refinement region of side 1.938 mm, where the cells have a square base of side 62.5 μm [25], being similar to the one used in the study [24] but with higher refinement. The mesh consists of a total number of 6M hexahedral cells with $157 \times 124 \times 292$ elements in the radial, azimuthal and axial directions, respectively, with an expansion ratio between elements of 1.01 in both the radius and the height.

MODELLING APPROACH

The numerical simulations of the reacting spray were conducted using the Lagrangian Particle Tracking (LPT) method for the dispersed-phase, while large-eddy simulation with a flamelet method is used to describe the gas phase. The liquid phase is described by a set of ordinary differential equations (ODEs) that provide the state of a droplet, location ($\vec{X}_p$), velocity ($\vec{U}_p$), temperature (T_p) and diameter (d_p). A kinematic modelling based on Schiller and Neumann [26] is used to describe particle motion, which is given by

$$\frac{d\vec{X}_p}{dt} = \vec{U}_p \tag{1}$$

$$\frac{d\vec{U}_p}{dt} = \frac{3C_D}{d_p}\frac{\bar{\rho}}{\rho_p}(\widetilde{\vec{u}} - \vec{U}_p)\,|\widetilde{\vec{u}} - \vec{U}_p|, \tag{2}$$

where $\bar{\rho}$ and ρ_p are the gas and particle densities, respectively, while $\widetilde{\vec{u}}$ is the gas velocity and C_D is the drag coefficient which is calculated as

$$C_D = \frac{24}{Re_p}\left(1 + \frac{Re_p^{2/3}}{6}\right), \tag{3}$$

with Re_p the Reynold number seen by the particle and defined as $\overline{\rho}\,|\widetilde{\vec{u}} - \vec{U}_p| d_p/\mu_m$ with μ_m the viscosity in the boundary layer near the droplet surface obtained from the 1/3 rule (in the following subscript m will denote properties computed according to the 1/3 rule).

The model proposed by Ambramzon and Sirignano [27] is used to account for droplet evaporation. Therefore, heat transfer effects between the droplet and the surroundings are accounted for by the Ranz-Marshall correlation for the calculations of the Sherwood (Sh) and Nusselt (Nu) numbers according to

$$Sh_m = 2 + 0.6\,Re_p^{1/2}\,Sc_m^{1/3}, \tag{4}$$

$$Nu_m = 2 + 0.6\,Re_p^{1/2}\,Pr_m^{1/3}, \tag{5}$$

with Sc and Pr being the Schmidt and Prandtl numbers, respectively. When evaporation is present Bird's correction is considered to account for the reduction of heat transfer.

The effect between the dispersed phase and the carrier phase comes from the two way coupling between both phases. This coupling is defined by imposing the source terms generated by drag, heat and mass exchange on the gas phase. The poly-disperse spray injection model is represented by a Rosin-Rammler distribution with a mean diameter of 1.5 μm and exponent $n = 2.7$.

The flow solver uses the low Mach number limit of the Navier-Stokes equations and the combustion model is based on the flamelet method [28]. The governing equations describing the gaseous phase include momentum, continuity and total enthalpy, along with governing equations for each of the control variables of the low-dimensional manifold. In terms of controlling variables, mixture fraction $\tilde{Z}$, its variance $\tilde{Z}_v$, progress variable $\tilde{Y}_c$ and normalised enthalpy $\tilde{i}$ are used to parametrize the thermochemical conditions of the flame with the flow field. Therefore in order to account for the subgrid effects of mixture fraction, an additional transport equation describing the subgrid variance of the mixture fraction $\widetilde{Z}_v$ is solved.

Mixture fraction is determined by Bilger's formula, while the progress variable Y_c is defined as $Y_c = 1/3(Y_{CO_2} + Y_{CO} + Y_{HO_2})$. The system of equations is given by:

$$\frac{\partial(\overline{\rho}\,\tilde{Z})}{\partial t} + \nabla\cdot\left(\overline{\rho}\,\tilde{\vec{u}}\,\tilde{Z}\right) = -\nabla\cdot\overline{\tau}_Z + \nabla\cdot\left(\bar{\rho}\,\bar{D}\,\nabla\tilde{Z}\right) + \bar{S}_Z, \tag{6}$$

$$\frac{\partial(\overline{\rho}\,\tilde{Y}_c)}{\partial t} + \nabla\cdot\left(\overline{\rho}\,\tilde{\vec{u}}\,\tilde{Y}_c\right) = -\nabla\cdot\overline{\tau}_{Y_c} + \nabla\cdot\left(\bar{\rho}\,\bar{D}\,\nabla\tilde{Y}_c\right) + \overline{\dot{\omega}}_{Y_c}, \tag{7}$$

where the unresolved terms appearing after the LES filtering $\overline{\tau}_Z$ and $\overline{\tau}_{Y_c}$ are closed using a gradient diffusion approach [29]. The

Vreman eddy-viscosity model has been adopted [30] using a constant $c_k = 0.1$. The same single-value constant has been used in previous studies and it is also retained here [31, 32]. The source term S_Z in the $\tilde{Z}$ equation refers to the mass generated by droplet evaporation, while $\overline{\dot{\omega}}_{Y_c}$ is the filtered progress variable source term, which is tabulated in the flame manifold. Finally, D is the diffusion mass coefficient.

Equation for mixture fraction variance reads:

$$\frac{\partial(\overline{\rho}\widetilde{Z}_v)}{\partial t} + \nabla\cdot\left(\overline{\rho}\,\tilde{\vec{u}}\widetilde{Z}_v\right) = -\nabla\cdot\overline{\tau}_{\widetilde{Z}_v} + \nabla\cdot\left(\bar{\rho}\bar{D}\nabla\widetilde{Z}_v\right) - \\ - 2\overline{\tau}_Z\cdot\nabla\tilde{Z} - 2\bar{s}_{\chi_Z}, \quad (8)$$

where $\bar{s}_{\chi_Z}$ is the unresolved part of the scalar dissipation rate and is modeled assuming a linear relaxation of the variance within the subgrid [29]. Finally, equation for the total enthalpy h reads

$$\frac{\partial(\overline{\rho}\widetilde{h})}{\partial t} + \nabla\cdot\left(\overline{\rho}\,\tilde{\vec{u}}\widetilde{h}\right) = -\nabla\cdot\overline{\tau}_{\widetilde{h}} + \nabla\cdot\left(\bar{\rho}\bar{D}\nabla\widetilde{h}\right) + \bar{S}_h, \quad (9)$$

where $\overline{\tau}_{\widetilde{h}}$ is the unresolved enthalpy flux, which is modelled also by a gradient diffusion approach [29] and $\bar{S}_h$ is the source term due to evaporation. To access to the manifold $\widetilde{h}$ is normalized according to the expression

$$i = \frac{\widetilde{h} - h_{min}(\widetilde{Z},\widetilde{Z}_v)}{h_{max}(\widetilde{Z},\widetilde{Z}_v) - h_{min}(\widetilde{Z},\widetilde{Z}_v)}, \quad (10)$$

where $h_{min}(\widetilde{Z},\widetilde{Z}_v)$ and $h_{min}(\widetilde{Z},\widetilde{Z}_v)$ are the minimum and maximum enthalpy, respectively, computed from the maximum heat loss and the adiabatic case.

The Turbulence-Chemistry Interaction (TCI) is accounted for by the Filtered Probability Density Functions (FPDFs), which depend on the set $(\widetilde{Z},\widetilde{Z}_v,\widetilde{Y}_c,\widetilde{i})$. Statistical independence is assumed among all four controlling variables. A beta function is adopted as FPDF for mixing variables $(\widetilde{Z},\widetilde{Z}_v)$, while Dirac's delta δ FPDF is used for the progress variable $\widetilde{Y}_c$ and normalized enthalpy $\widetilde{i}$.

Regarding the numerical algorithms, the governing equations are solved using a low dissipation numerical scheme based on a third order explicit Runge-Kutta scheme for momentum and scalars, with a second order spatial discretization using linear finite elements [31]. The numerical simulations were conducted with the multiphysics code Alya developed at BSC [33].

FLAMELET GENERATION

The combustion process is described by the use of tabulated diffusion flamelets at varied strain using a low-dimensional manifold based on the flamelet method. This method has been chosen since it has been shown to be suitable for diesel-like sprays modelling [24, 34]. The chemistry is described by two different reaction mechanisms, a skeletal mechanism from Yao et el. [35] widely used in the ECN for dodecane and [13] for OMEx.

For each enthalpy level, the autoigniting process of a single laminar flame at at a fixed strain rate $a = 500$ 1/s is computed [28], while the rest of the manifold is filled with the steady flamelet solutions from the counterflow diffusion flame (S-curve). After the flamelet generation, a thermochemical database with the gas properties is parametrized in terms of mixture fraction Z, progress variable Y_c and normalized enthalpy i. Such database is integrated based on the FPDFs to obtain a manifold that contains the turbulent variables. The manifold is discretized in 101, 11, 501 and 5 values for $\widetilde{Z}$, $\widetilde{Z}_v$, $\widetilde{Y}_c$ and $\widetilde{i}$, respectively. The discretization was chosen as a balance between accuracy and memory limitations. The computation of single one-dimensional flames is obtained from the code Ember [36], while the flamelet tabulation and FPDF integration are done from the in-house Python-based tool FlameGen [37].

THERMOCHEMICAL STRUCTURE OF THE FLAME

In this section, a preliminary analysis of the flame structure is carried out through the inspection of the ignition of the two fuels under nominal spray A conditions. The analysis is conducted by the evaluation of the unsteady evolution of an auto-igniting flamelet at a fixed strain ($a = 500\,s^{-1}$). Figure 1 shows these profiles for dodecane and OMEx using a counterflow diffusion flame configuration. Taking into account the differences in stoichiometric mixture fraction, the two fuels show a similar flame structure during ignition, starting the oxidation on very lean mixtures, with a subsequent slow down of reactivity during the the cool flame, which may produce increments in temperature around 150 K for some mixtures, after the first ignition [9, 22]. Such reduction of reactivity allows that ignition propagates towards richer mixtures while a wide range of mixtures remains frozen due to the long period of the cool flame. Then, after reaching a rich mixture with equivalence ratio ϕ around 2, the high temperature chemistry triggers chemical reactions (second ignition) and combustion mainly occurs at one fixed mixture fraction (most reactive mixture fraction Z_{MR}), as shown by the dashed line in Fig. 1. The rapid production of radicals and heat release generates intense diffusion fluxes from Z_{MR} to its leaner and richer mixture vicinity [22, 38] which in turn allow to overcome the cool flame period in these mixtures and start their second ignition. Subsequently, the mixture fraction that acted as the most reactive (0.10 for dodecane and 0.19 for OMEx) suffers a decrease in reactivity, around 1300 K for dodecane and 1600 K for OMEx, provoking

a displacement to leaner mixtures of the most reactive mixture until reaching stoichiometry.

Even if the ignition process is very similar for the two fuels from a qualitative point of view, there exist important differences regarding the shift towards higher mixtures in the case of OMEx due to its larger stoichiometric mixture fraction value, caused by its content in oxygen, and the different range of temperatures where the richest most reactive mixture fraction leads ignition. Finally, another noticeable difference is the milder temperature increase during the lean ignition phases of OMEx compared to dodecane, which is a result of a not so prominent cool flame behaviour. It is worth mentioning that even if the quantitative evolution of the flame may be affected by the choice of the mechanism [22], the qualitative picture of ignition is expected to be accurate considering the agreement with experiments in subsequent results.

The ignition process can be better understood analysing the chemical source term of the progress variable, $\dot{\omega}_{Y_c} = \dot{\omega}_{Y_c}(Z,c)$ where c is the normalized progress variable Y_c, that corresponds to the previous laminar flames and is shown in Fig. 2. This source term is used in equation 7 after integrating with the FPDF. While for dodecane a region of intermediate values for $\dot{\omega}_{Y_c}$ is found at relatively low values of the progress variable, which correspond to the first steps of the ignition, and the highest source terms occur in a very narrow region close to the stoichiometric at very high values of the progress variable, for the OMEx no intense source terms are detected at the first period of ignition while the highest source terms are observed in the vicinity of the richest Z_{MR} (0.2) in a relatively wide region and only intermediate values are found again close to Z_{st}. The position of the peak values for $\dot{\omega}_{Y_c}$ are clearly in correspondence with the evolution of the flame ignition shown in Fig. 1.

Finally, the profiles of acetylene (C_2H_2) as a function of the mixture fraction for the one-dimensional steady laminar flames are shown in figure Fig. 3 for the two fuels under investigation. Acetylene is the first soot precursor and hence, its analysis can give a measure of the potential of oxygenated fuels, such as OMEx, to reduce soot emissions. As shown in figure 3, acetylene is only found at rich mixtures with the maximum mass fraction at an equivalence ratio of 2.5 for both fuels. The maximum mass fraction is reduced when increasing the strain rate but with a remarkable lower sensitivity for OMEx than for dodecane. The values for acetylene are one order of magnitude lower for the OMEx flames compared to those of dodecane, anticipating a drastic reduction of C_2H_2 mass production in the turbulent spray. Moreover, the convex shape of the profiles at Z=0.42 for OMEx shows that there is chemical consumption of acetylene at these very high equivalence ratios, which in turn, provokes that the mass fractions for C_2H_2 fall much faster that would happen if the profiles were similar to those of dodecane. These effects contribute to have lower production of soot precursors. However, this aspect may have no effect on the turbulent spray since, due

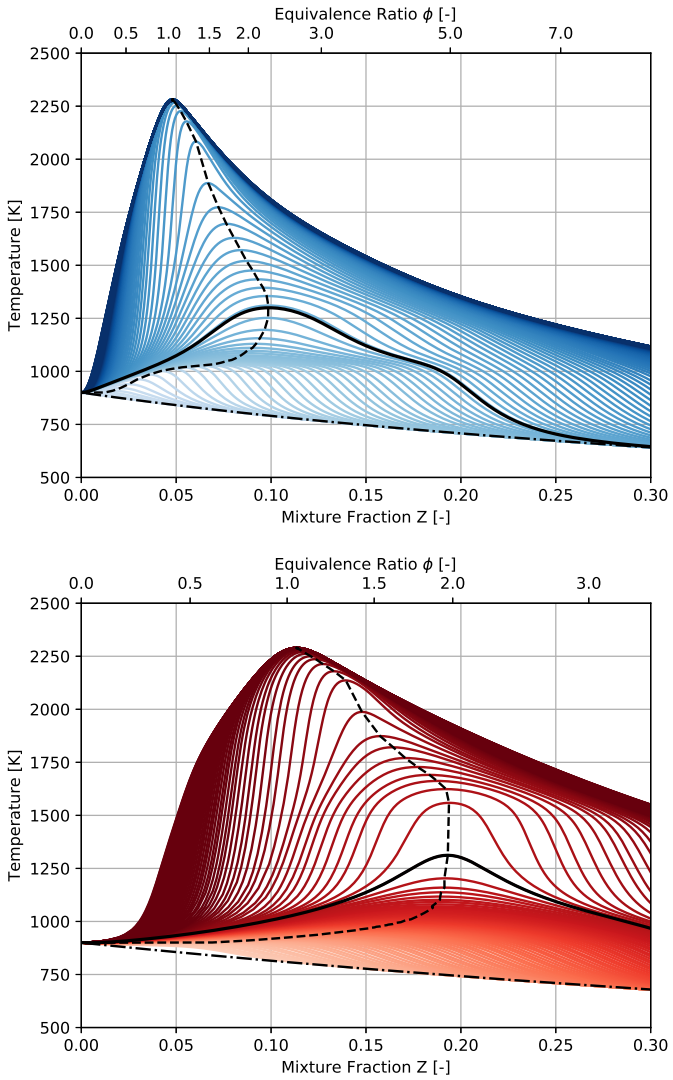

FIGURE 1: Temporal evolution for dodecane (top), OME_x (bottom). Vertical line represents stoichiometric mixture fraction, dashed line the evolution of most reactive mixture fraction and the solid line the flamelet with maximum temperature equal to 1300 K (see ECN ignition delay definition).

to the residence times of the spray, the thermochemical states of these very rich mixtures are found practically at inert conditions, as will be observed in next sections, what prevents the formation of precursors.

SPRAY-FLAME ASSESSMENT

This section shows a validation of the predictions of the modelling tools in terms of characteristic spray and combustion metrics. The simulations are compared with a recent experimen-

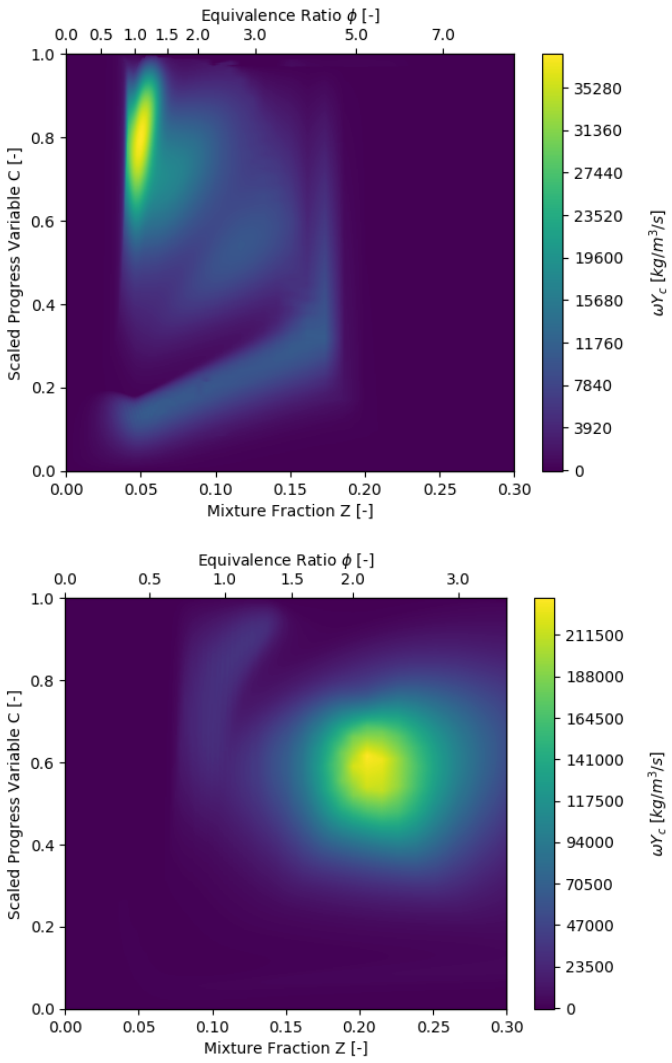

FIGURE 2: Chemical source term $\dot{\omega}_{Y_c}$ as a function of the mixture fraction and the normalized progress variable for dodecane (top) and OMEx (bottom).

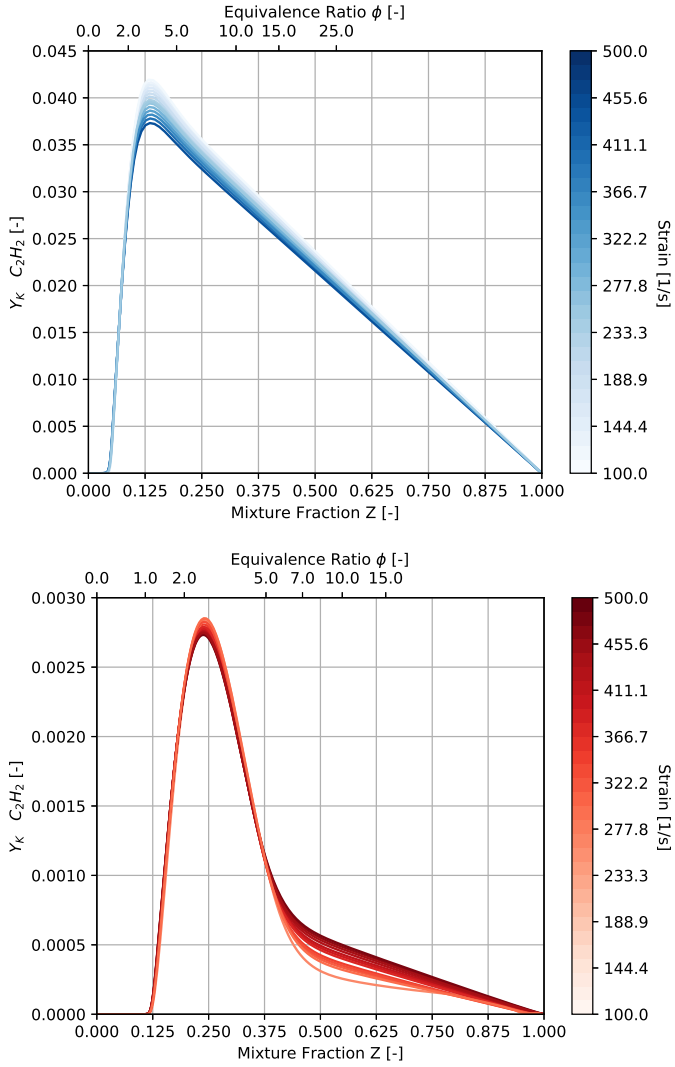

FIGURE 3: Acetylene mass fraction profiles versus mixture fraction for one-dimensional steady laminar flames for strain rates ranging from 100 to 500 1/s for dodecane (top) and OMEx (bottom).

tal database of renewable fuels generated in the high-pressure high-temperature vessel from CMT-Motores Térmicos [10, 11]. The experimental database contains spray diagnostics based on high-speed Schlieren, Diffuse Back-Illuminated (DBI), OH* chemiluminescence and Natural Luminosity (NL) imaging [10], as well as planar Laser-Induced Fluorescence (PLIF) of OH radical and formaldehyde (CH_2O) [11].

The tip penetration and the liquid length for the two sprays are shown in Fig. 4. Following the ECN guidelines, the tip penetration is defined as the distance from the nozzle projected on the axis to the most distant point with $\widetilde{Z} = 0.001$, while the liquid length is the distance from the nozzle projected on the axis with 95% of the liquid enclosed. The results show good correlation for the liquid length for both fuels, which is quite similar due to not very different volatility properties. The same injection condition, calibrated for dodecane, was retained for the two fuels for the sake of comparison, although it is expected that the primary breakup is slightly different. The spray tip penetration also shows an overall good agreement though it is slightly under-predicted for OMEx.

The validation is continued by comparing the ignition delay (ID) and lift-off length (LOL) for the experiments and simulations. For the simulations, ID is defined as the time spent from

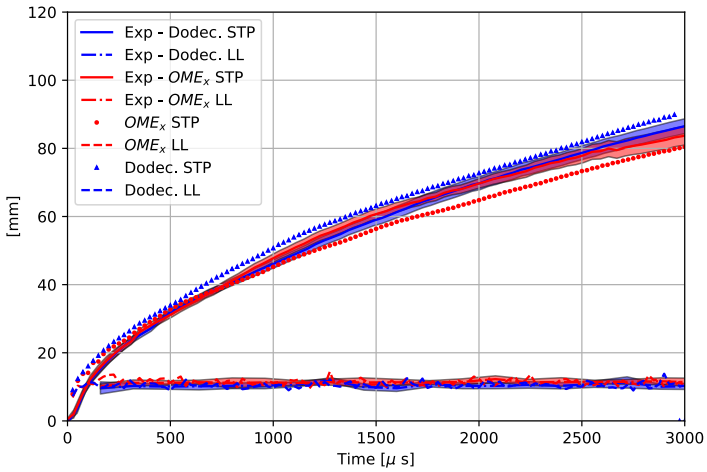

FIGURE 4: Comparison between experiments and LES for the spray tip penetration (STP) and liquid length (LL) for the two fuels. Uncertainty of measurements is delimited with shadowed regions.

start of injection (SOI) until the maximum temperature reaches the ambient temperature plus 400 K (1300 K), while the LOL is defined as the minimum distance from the nozzle projected on the axis to the point where 14% of the maximum instantaneous OH value in the domain is reached. The values for ID and LOL for the two fuels are presented in Table 1, showing good agreement between experiments and simulations, though an under-prediction of the ignition delay is found with the Yao et al. [35] mechanism for dodecane, as reported in the literature [22].

	ID (μs)	LOL (mm)	LL (mm)
Dodec. - Exp	432	18.89	10.0
Dodec. - LES	360	15.78	10.25
OMEx- Exp	323	19.33	11.6
OMEx- LES	306	22.67	11.2

TABLE 1: Ignition delay (ID), lift-off length (LOL) and liquid length (LL) for dodecane and OMEx with experiments and simulations.

QUASI-STEADY FLAME REGIME

This section deals with the analysis of the quasi-steady flame regime, to better understand the distribution of species and their role on the flame characteristics. A qualitative comparison of the tracer species for low and high temperature combustion are shown in Fig. 5 and 6 for dodecane and OMEx, respectively. A superposition of CH_2O and OH PLIF ensemble-averaged signals is presented and compared to azimuthally-averaged mass fractions as predicted from CFD.

In the case of dodecane, CH_2O from simulations is the first species to be observed starting from the nozzle, which extends further downstream and is eventually enclosed in-between the two OH lobes at the lift-off distance. CH_2O is consumed in this region due to the existence of the transition to high temperature reactions, as confirmed by the OH presence. Further downstream, OH is distributed along the stoichiometric reacting surface up to the spray tip. LIF measurements mainly confirm the simulated OH distribution, while CH_2O is not observed at the flame base mainly due to lasersheet attenuation as a consequence of the presence of soot and the spray head-on illumination configuration, as discussed in [11].

For OMEx, the numerical results show that both species are located similarly to dodecane and in agreement with experiments. The CH_2O is found upstream of OH, but the radial distribution is quite different. CH_2O cloud is narrower and fully disappears at the location where OH appears, with very little overlap, i.e. they are sequential in axial distribution. OH location is highly affected by the oxygenated character of the fuel and the corresponding location of the reacting front. As the stoichiometric mixture fraction is around a factor of 2 higher compared to dodecane, the stoichiometric surface will be narrower and much closer to the orifice. This pushes both OH lobes much closer to each other, as observed both in simulations and experiments, and they merge on the axis at an axial distance of around 65 *mm*. Regarding the low intensity of the experimental OH signal for OMEx between 65 and 80 mm, a more detailed study with a modified LIF setup has shown that it was most probably caused by OH* chemiluminescence interference. At the particular timing for Fig. 6, the tip penetration is found almost at 80 *mm* for both fuels (Fig. 4), but while OH fully reaches the tip of the jet for dodecane (Fig. 5), the OH disappears further upstream in the case of OMEx, see Fig. 6, meaning that the reaction front has reached a fully steady state.

Instantaneous temperature fields are shown in figure 7 together with the iso-contour for the stoichiometric mixture fraction. The previously discussed differences in key species are confirmed here in terms of temperature. For dodecane, temperature distribution is typical of a lifted hydrocarbon diffusion flame, with a radially displaced stoichiometric surface along which the reaction front is stabilized and, consequently, temperature achieves the peak values. Due to the larger air mass needed to achieve stoichiometry, the reaction front is not axially stabilized, and it progresses further downstream together with the tip of the jet, consistent with the previous discussion for OH distribution.

For OMEx, however, the stoichiometric surface is much narrower and shorter, due to the lower air needed to achieve stoichiometry, and this surface reaches the spray axis well upstream of the tip of the jet at around 65 mm, consistent with the location

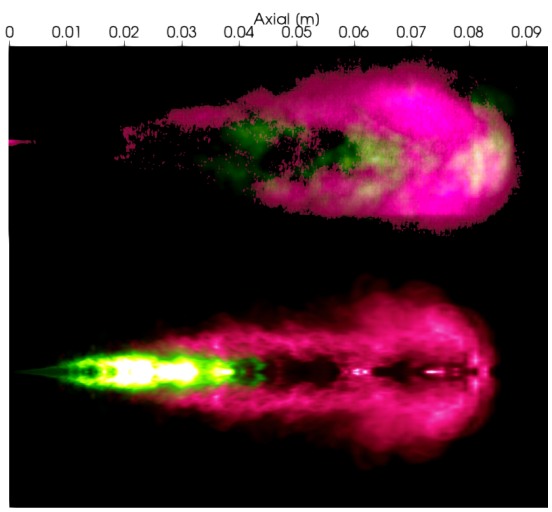

FIGURE 5: Comparison of OH (in purple) and CH_2O (in green) distribution for dodecane at 2600 μs. Experimental planar LIF intensity (top), CFD-derived azimuthally-averaged species mass fraction (bottom).

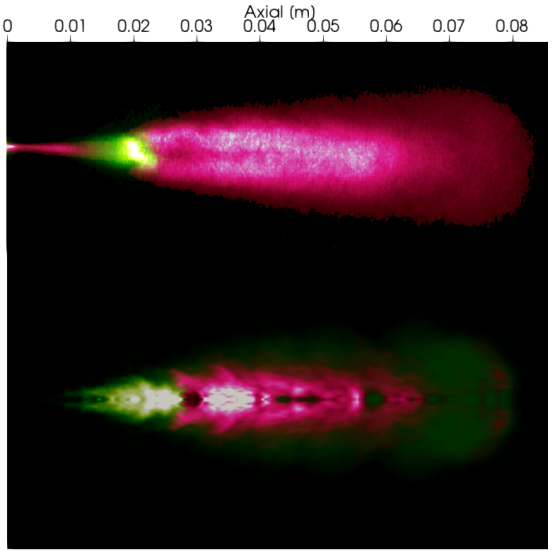

FIGURE 6: Comparison of OH (in purple) and CH_2O (in green) distribution for OME_X at 2600 μs. Experimental planar LIF intensity (top), CFD-derived azimuthally-averaged species mass fraction (bottom).

where the latest OH was found. Even though peak temperature values are also found on this surface, a high temperature zone is also observed further downstream, due to the presence of hot combustion products which become diluted before reaching the jet tip.

Finally, mixture fraction - temperature maps for the previous timing for both fuels are shown in Fig. 8, where only points with species mass fraction above a threshold of 10% have been included. Moreover, the value of mass fraction is denoted by the level of transparency, while the iso-contours of density of the cloud of points have been included for reference. This map merges information from Figs. 5, 6 and 7 into a more quantitative single plot. Dodecane shows the well-known distribution, with high temperature flame equilibrium values up to a mixture fraction of 0.11 (equivalence ratio slightly higher than 2.5) [22]. Consistent with previous observations and analysis, OH is mostly found around the stoichiometric high-temperature location with a similar distribution in both the lean and the rich mixtures, while CH_2O is present for rich mixtures and low and intermediate temperatures.

In agreement with the flamelet discussion above and the higher stoichiometric mixture fraction, the observed structure for OMEx is different. The reacting region is shifted towards higher mixture fraction values, however, the high flame equilibrium temperatures are confined to lower equivalence ratios (up to 1.6) and at $Z = 0.17$ such flame equilibrium temperatures suffer a very abrupt slope evidencing that the flame is globally much leaner. Regarding the species, and differently from the case of dodecane, OH extends mainly in the region of lean mixtures while a very low proportion of the population is found at rich mixtures and CH_2O is present in a broad range of mixture fraction values up to 0.25. Moreover, most of the points for OH are very close to the flame equilibrium temperature, as seen in Fig.7, while the vast majority of points with representative mass fractions for CH_2O are close to the mixing line and with temperatures lower than 1300 K. This demonstrates that there is a clear separation without overlapping between the spatial regions occupied by these species. Such separation is not observed for the case of dodecane where the species extend in wider regions in the mixture fraction-temperature map, with a cloud of points for OH found in both lean and rich sides at high temperatures but relatively far from the equilibrium and CH_2O reaching temperatures as high as 1700 K, and points may be found much closer. This is also consistent with the difference in low temperature behaviour between both fuels observed in Fig. 2.

Finally, it is worth mentioning, that a reduction of two orders of magnitude in the total mass of acetylene in the CFD domain for the turbulent spray is observed when going from dodecane to OMEx which, in turn, is expected to strongly reduce the soot formation in OMEx spray flames. This is in agreement with results from Fig. 3 as well as experimental measurements, for which no soot formation was observed for OMEx at the current operating conditions [11].

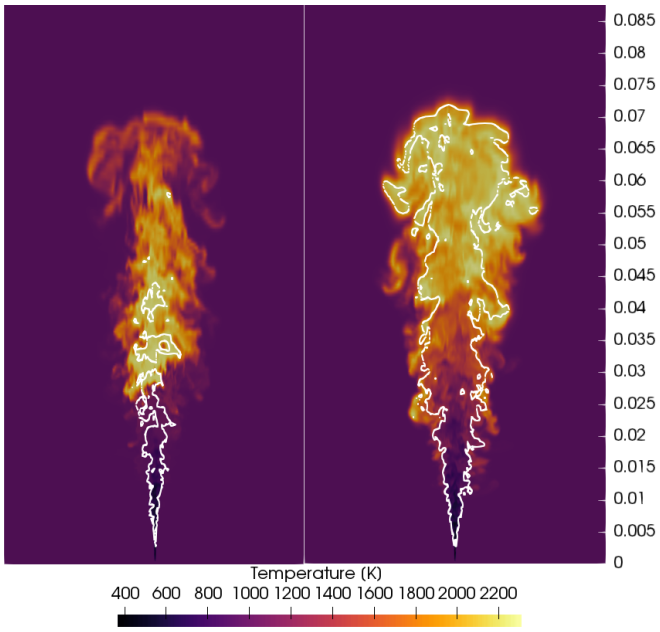

FIGURE 7: Instantaneous temperature for OMEx (left) and dodecane (right) at 2.5 ms. White line corresponds to stoichiometric mixture fraction. Scale is in meters.

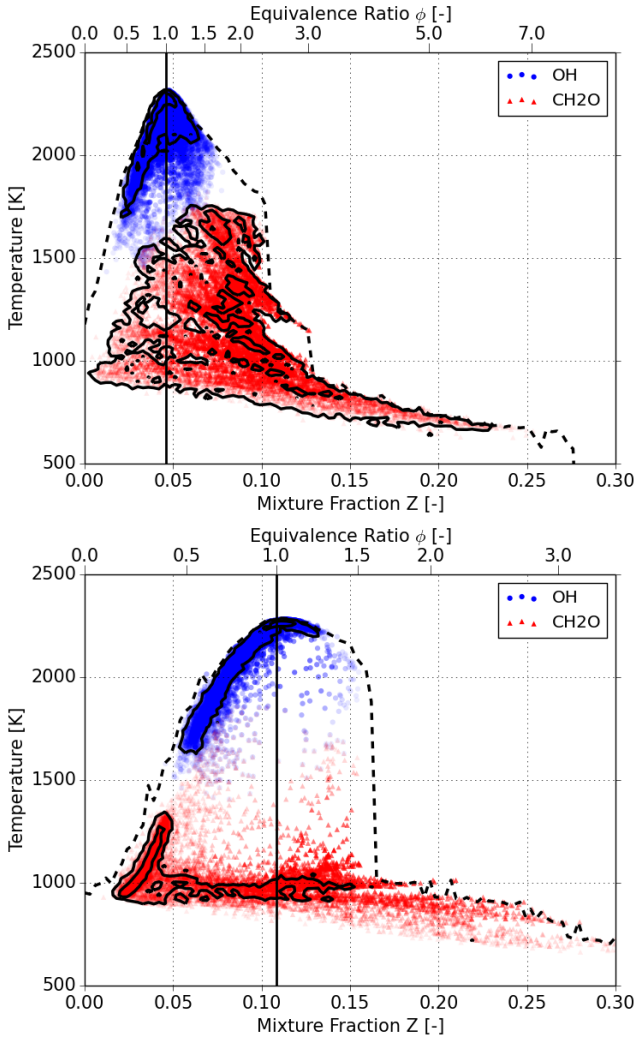

FIGURE 8: Mixture fraction-temperature map at quasi-steady regime for dodecane (top) and OMEx (bottom). Only points with $Y_i > 0.1 * Y_{i,max}$, with $Y_{i,max}$ the maximum mass fraction for species i, are represented. The mass fraction is denoted by the transparency level being maximum at $Y_{i,max}$. Level curves for the density of points in the map are shown for 5 and 40% of the maximum density for each species. Dashed line indicates the maximum temperature as a function of the mixture fraction found in the spray. Vertical line is placed at the stoichiometric mixture fraction.

CONCLUSIONS

Oxymethylene ethers represent a possible solution in the decarbonization path of the transportation sector, which may also help to meet restrictions in soot production imposed by the regulations without altering the engine architecture due to their similar properties to diesel fuel. In this work the flame structure for these fuels has been analysed by means of LES simulations and compared to dodecane under the Spray A condition from the Engine Combustion Network.

First, the igniting laminar flamelets have helped describe chemical reaction steps. The role of the cool flame has been highlighted to explain how the first ignition kernels are located at lean mixtures and subsequently frozen allowing the propagation of combustion towards the rich mixtures. Differences between both fuels are evident in terms of stochiometry, as well as the intensity of the low temperature period, with OMEx exhibiting an initially milder temperature increase due to the lower reactivity for low progress variable values. For OMEx, the most reactive mixture fraction corresponds to a leaner equivalence ratio compared to dodecane.

In a second step, LES simulations have been assessed by their direct comparison to experimental results in terms of spray tip penetration, liquid length, ID and LOL. All combustion metrics are adequately predicted by the simulation framework. The quasi-steady flame has been described in both physical space and mixture fraction-temperature maps. Compared to dodecane, combustion in OMEx is not only displaced to leaner mixtures, but there exists an accentuated separation in low and high temperature species location (CH_2O and OH, respectively) caused by the different chemical behaviour. Moreover, a strong reduction in the production of acetylene in the turbulent spray has been observed pointing out the potential of oxygenated fuels to avoid

the formation of soot. Finally, OMEx reaction front stabilizes within the injection period, resulting in a much shorter diffusion flame compared to dodecane.

ACKNOWLEDGMENT

The research leading to these results has received funding through the ENERXICO project from the European Union's Horizon 2020 Programme, grant agreement n° 828947, and from the Mexican Department of Energy, CONACYT-SENER Hidrocarburos grant agreement n° B-S-69926 and the Spanish Ministry of Economy and Competitiveness in the frame of the CHEST project (TRA2017-89139-C2-2-R). Furthermore, computer resources and technical assistance has been provided by the Red Española de Supercomputación (RES) (IM-2021-1-00214, IM-2020-3-0029, IM-2020-2-0023,IM-2020-1-0013).

REFERENCES

[1] Agarwal, A. K., Singh, A. P., and Maurya, R. K., 2017. "Evolution, challenges and path forward for low temperature combustion engines". *Progress in energy and combustion science,* ***61***, pp. 1–56.

[2] Brynolf, S., Taljegard, M., Grahn, M., and Hansson, J., 2018. "Electrofuels for the transport sector: A review of production costs". *Renewable and Sustainable Energy Reviews,* ***81***, pp. 1887–1905.

[3] Lumpp, B., Rothe, D., Pastötter, C., Lämmermann, R., and Jacob, E., 2011. "Oxymethylene ethers as diesel fuel additives of the future". *MTZ worldwide eMagazine,* ***72***(3), pp. 34–38.

[4] Awad, O. I., Ma, X., Kamil, M., Ali, O. M., Ma, Y., and Shuai, S., 2020. "Overview of polyoxymethylene dimethyl ether additive as an eco-friendly fuel for an internal combustion engine: Current application and environmental impacts". *Science of The Total Environment,* ***715***, p. 136849.

[5] Dworschak, P., Berger, V., Härtl, M., and Wachtmeister, G., 2020. Neat oxymethylene ethers: Combustion performance and emissions of OME 2, OME 3, OME 4 and OME 5 in a single-cylinder diesel engine. Tech. rep., SAE Technical Paper.

[6] Pélerin, D., Gaukel, K., Härtl, M., Jacob, E., and Wachtmeister, G., 2020. "Potentials to simplify the engine system using the alternative diesel fuels oxymethylene ether OME1 and OME3-6 on a heavy-duty engine". *Fuel,* ***259***, jan, p. 116231.

[7] Omari, A., Heuser, B., and Pischinger, S., 2017. "Potential of oxymethylenether-diesel blends for ultra-low emission engines". *Fuel,* ***209***(July), pp. 232–237.

[8] Iannuzzi, S. E., Barro, C., Boulouchos, K., and Burger, J., 2017. "POMDME-diesel blends: Evaluation of performance and exhaust emissions in a single cylinder heavy-duty diesel engine". *Fuel,* ***203***, pp. 57–67.

[9] Goeb, D., Davidovic, M., Cai, L., Pancharia, P., Bode, M., Jacobs, S., Beeckmann, J., Willems, W., Heufer, K. A., and Pitsch, H., 2020. "Oxymethylene ether–n-dodecane blend spray combustion: Experimental study and large-eddy simulations". *Proceedings of the Combustion Institute*.

[10] Pastor, J. V., García-Oliver, J. M., Micó, C., García-Carrero, A. A., and Gómez, A., 2020. "Experimental study of the effect of hydrotreated vegetable oil and oxymethylene ethers on main spray and combustion characteristics under engine combustion network spray a conditions". *Applied Sciences,* ***10***(16), p. 5460.

[11] Pastor, J. V., Garcia-Oliver, J. M., Micó, C., and Tejada, F. J., 2020. Comparison of the diffusive flame structure for dodecane and OME X fuels for conditions of spray A of the ECN. Tech. rep., SAE Technical Paper.

[12] Jacobs, S., Döntgen, M., Alquaity, A. B., Kopp, W. A., Kröger, L. C., Burke, U., Pitsch, H., Leonhard, K., Curran, H. J., and Heufer, K. A., 2019. "Detailed kinetic modeling of dimethoxymethane. Part II: Experimental and theoretical study of the kinetics and reaction mechanism". *Combustion and Flame,* ***205***, jul, pp. 522–533.

[13] Cai, L., Jacobs, S., Langer, R., vom Lehn, F., Heufer, K. A., and Pitsch, H., 2020. "Auto-ignition of oxymethylene ethers (OMEn, n= 2–4) as promising synthetic e-fuels from renewable electricity: shock tube experiments and automatic mechanism generation". *Fuel,* ***264***, p. 116711.

[14] Benajes, J., García-Oliver, J., Pastor, J., and de León-Ceriani, D., 2020. A computational study on OME1 spray combustion under ECN spray A conditions. Tech. rep., ILASS Asia Paper.

[15] Pickett, L. M., Bruneaux, G., and Payri, R., 2020. "Engine combustion network". *Sandia National Laboratories, Livermore, CA, https://ecn.sandia.gov/.*

[16] Payri, R., García-Oliver, J. M., Xuan, T., and Bardi, M., 2015. "A study on diesel spray tip penetration and radial expansion under reacting conditions". *Applied Thermal Engineering,* ***90***, pp. 619–629.

[17] Skeen, S. A., Manin, J., and Pickett, L. M., 2015. "Simultaneous formaldehyde PLIF and high-speed schlieren imaging for ignition visualization in high-pressure spray flames". *Proceedings of the Combustion Institute,* ***35***(3), pp. 3167–3174.

[18] Maes, N., Meijer, M., Dam, N., Somers, B., Toda, H. B., Bruneaux, G., Skeen, S. A., Pickett, L. M., and Manin, J., 2016. "Characterization of spray A flame structure for parametric variations in ECN constant-volume vessels using chemiluminescence and laser-induced fluorescence". *Combustion and Flame,* ***174***, pp. 138–151.

[19] Tagliante, F., Malbec, L. M., Bruneaux, G., Pickett, L. M., and Angelberger, C., 2018. "Experimental study of the

stabilization mechanism of a lifted diesel-type flame using combined optical diagnostics and laser-induced plasma ignition". *Combustion and Flame,* ***197***, pp. 215–226.

[20] Blomberg, C. K., Zeugin, L., Pandurangi, S. S., Bolla, M., Boulouchos, K., and Wright, Y. M., 2016. "Modeling split injections of ECN "Spray A" using a conditional moment closure combustion model with RANS and LES". *SAE International Journal of Engines,* ***9***(4), pp. 2107–2119.

[21] Pei, Y., Hawkes, E. R., Bolla, M., Kook, S., Goldin, G. M., Yang, Y., Pope, S. B., and Som, S., 2016. "An analysis of the structure of an n-dodecane spray flame using TPDF modelling". *Combustion and Flame,* ***168***, pp. 420–435.

[22] Payri, F., García-Oliver, J. M., Novella, R., and Pérez-Sánchez, E. J., 2019. "Influence of the n-dodecane chemical mechanism on the cfd modelling of the diesel-like ecn spray a flame structure at different ambient conditions". *Combustion and Flame,* ***208***, pp. 198–218.

[23] Xuan, T., Desantes, J. M., Pastor, J. V., and Garcia-Oliver, J. M., 2019. "Soot temperature characterization of spray a flames by combined extinction and radiation methodology". *Combustion and Flame,* ***204***, pp. 290–303.

[24] Desantes, J., García-Oliver, J., Novella, R., and Pérez-Sánchez, E., 2020. "Application of a flamelet-based CFD combustion model to the les simulation of a diesel-like reacting spray". *Computers & Fluids,* ***200***, p. 104419.

[25] Senecal, P., Pomraning, E., Richards, K., and Som, S., 2013. An investigation of grid convergence for spray simulations using an les turbulence model. Tech. rep., SAE Technical Paper.

[26] Schiller, L., and Naumann, Z., 1935. "A drag coefficient correlation". *Z. Ver. Deutsch. Ing.*, pp. 77–318.

[27] Abramzon, B., and Sirignano, W. A., 1989. "Droplet vaporization model for spray combustion calculations". *International journal of heat and mass transfer,* ***32***(9), pp. 1605–1618.

[28] Wehrfritz, A., Kaario, O., Vuorinen, V., and Somers, B., 2016. "Large eddy simulation of n-dodecane spray flames using flamelet generated manifolds". *Combustion and Flame,* ***167***, pp. 113–131.

[29] Domingo, P., Vervisch, L., and Veynante, D., 2008. "Large-eddy simulation of a lifted methane jet flame in a vitiated coflow". *Combustion and Flame,* ***152***(3), pp. 415–432.

[30] Vreman, A. W., 2004. "An eddy-viscosity subgrid-scale model for turbulent shear flow: Algebraic theory and applications". *Physics of Fluids,* ***3670***(16).

[31] Both, A., Lehmkuhl, O., Mira, D., and Ortega, M., 2020. "Low-dissipation finite element strategy for low mach number reacting flows". *Computers & Fluids,* ***200***, p. 104436.

[32] Mira, D., Lehmkuhl, O., Both, A., Stathopoulos, P., Tanneberger, T., Reichel, T. G., Paschereit, C. O., Vázquez, M., and Houzeaux, G., 2020. "Numerical characterization of a premixed hydrogen flame under conditions close to flashback". *Flow, Turbulence and Combustion,* ***104***(2), pp. 479–507.

[33] Vázquez, M., Houzeaux, G., Koric, S., Artigues, A., Aguado-Sierra, J., Arís, R., Mira, D., Calmet, H., Cucchietti, F., Owen, H., et al., 2016. "Alya: Multiphysics engineering simulation toward exascale". *Journal of computational science,* ***14***, pp. 15–27.

[34] Kahila, H., Wehrfritz, A., Kaario, O., Masouleh, M. G., Maes, N., Somers, B., and Vuorinen, V., 2018. "Large-eddy simulation on the influence of injection pressure in reacting spray A". *Combustion and Flame,* ***191***, pp. 142–159.

[35] Yao, T., Pei, Y., Zhong, B.-J., Som, S., Lu, T., and Luo, K. H., 2017. "A compact skeletal mechanism for n-dodecane with optimized semi-global low-temperature chemistry for diesel engine simulations". *Fuel,* ***191***, pp. 339–349.

[36] Long, A. E., Speth, R. L., and Green, W. H., 2018. "Ember: An open-source, transient solver for 1D reacting flow using large kinetic models, applied to strained extinction". *Combustion and Flame,* ***195***, pp. 105–116.

[37] Both, A., Surapaneni, A., and Mira, D., 2020. "Flamegen". *https://gitlab.com/bothambrus/flamegen*.

[38] Krisman, A., Hawkes, E. R., and Chen, J. H., 2019. "A parametric study of ignition dynamics at ECN Spray A thermochemical conditions using 2D DNS". *Proceedings of the Combustion Institute,* ***37***(4), pp. 4787–4795.